Volume 10 | Number 47 | 21 December 2014 | Pages 9375–9586

Soft Matter

www.softmatter.org

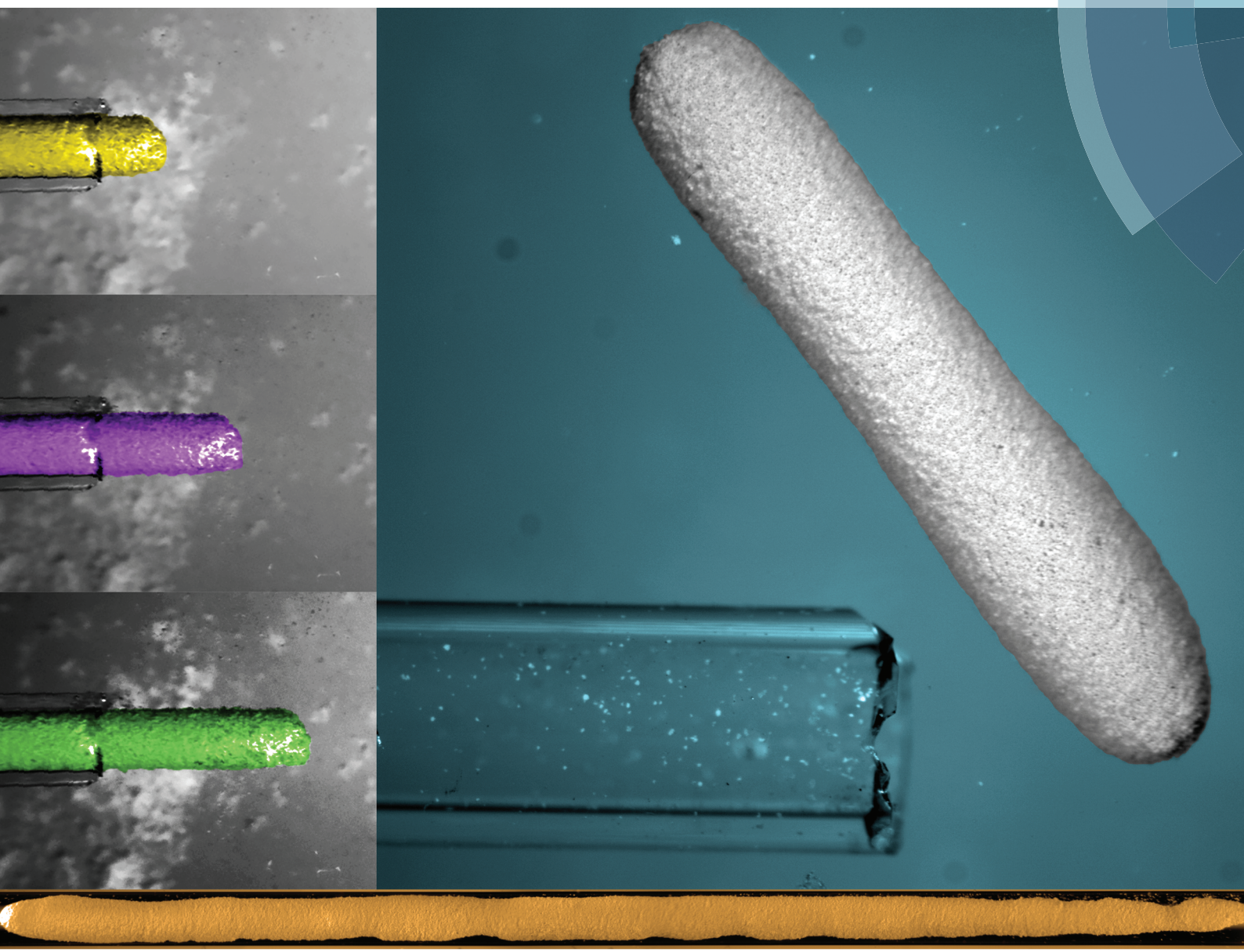

ISSN 1744-683X

ROYAL SOCIETY OF CHEMISTRY

PAPER
Farzam Zoueshtiagh, Michael Baudoin and David Guerrin
Capillary tube wetting induced by particles: towards armoured bubbles tailoring

Soft Matter

PAPER

View Article Online
View Journal | View Issue

CrossMark click for updates

Cite this: *Soft Matter*, 2014, **10**, 9403

Capillary tube wetting induced by particles: towards armoured bubbles tailoring†

Farzam Zoueshtiagh,‡* Michael Baudoin‡* and David Guerrin

Received 25th July 2014
Accepted 10th September 2014

DOI: 10.1039/c4sm01648c

www.rsc.org/softmatter

In this paper, we report on the strongly modified dynamics of a liquid finger pushed inside a capillary tube, when partially wettable particles are lying on the walls. Particles promote the appearance of new regimes and enable the tailored synthesis of bubbles encapsulated in a monolayer of particles (so-called "armoured bubbles"). This remarkable behavior arises due to the collection of particles at the air–liquid interface, which modify the global energy balance and stabilize the interface. Armoured-bubbles are of primary interest in industrial processes since they display increased stability, interfacial rigidity and can even sustain non-spherical shapes. This work opens perspective for a low cost bubbles-on-demand technology enabling the synthesis of armoured bubbles with specific sizes, shapes and composition.

Published on 11 September 2014. Downloaded by Univ Lille 1 on 05/02/2015 13:44:30.

1 Introduction

Particle covered interfaces between immiscible fluids are of primary interest in a wide variety of industrial, medical and technological applications: stabilization of bubbly liquids, foams and emulsions,[1–4] flotation-based extraction and separation processes,[5] drug encapsulation,[6] food processing[7] or even surface nanostructuring.[8] Particles drastically alter the behavior of interfaces and make them display solid-like behavior[9] such as interfacial elasticity, buckling instability[10] or cracks formation.[11] When droplets or bubbles are encapsulated in such hybrid interfaces, the "armour" surrounding them strongly modifies their interaction with their environment: Droplets encapsulated inside a layer of partially wettable particles (so-called "liquid marbles") do not wet substrates,[12] thereby suppressing dissipation at the contact line, and also become more stable toward coalescence with other drops.[13] Their bubble counterpart, the "armoured bubbles", have the singular property of sustaining stable non-spherical shape due to the jamming of particles covering their surface.[14] They also exhibit increased stability toward dissolution since they naturally evolve into faceted polyhedral shapes that make the Laplace overpressure vanish.[15] While it has been shown that microfluidic and chemical techniques[16–20] allow the production of spherical droplets with colloidal armour, the tailored production of armoured bubbles with non-spherical shapes, controlled size and composition remains a challenge.

In this paper, we study the dynamics of liquid fingers pushed inside particle-covered capillary tubes. The propagation of liquid fingers in capillary tubes has been largely studied since the early work of Bretherton,[21] Hoffman[22] and Tanner.[23] However, particles have not been considered as a way of modifying the meniscus dynamics and promoting the emergence of new regimes. Bretherton had shown that air blown inside a liquid-filled capillary tube results in the formation of an air finger through the deposition of a liquid film on the walls behind the meniscus. Here we show that the presence of particles on the walls can lead to the mirror situation wherein liquid pushed inside a capillary tube filled with air results in the deposition of a liquid film ahead of the meniscus. This liquid film is covered and stabilized by a single monolayer of closed packed particles. Their jamming prevents the development of Rayleigh-Plateau instability and allows the formation of an encapsulated gas finger with large aspect ratio. This gas finger eventually collapses into an armoured bubble (see Fig. 1) due to an increase of the resistance of the bubbly finger to motion. This system therefore enables the synthesis of armoured bubbles, whose shape and size is prescribed by the geometry of the capillary tube.

Since the appearance of this new regime depends on the global surface energy balance, we investigate here the influence of the wetting properties of the walls and the particles on the evolution of the meniscus. A model is developed and provides a criterion for the formation of armoured bubbles.

2 Materials and methods

2.1 Experimental setup

A liquid finger is either pushed at constant flow rate $Q = 3$ μl min^{-1} with a syringe pump, or at constant pressure head $\Delta P = 0.2$ kPa with a syphon system inside a glass

International Laboratory LEMAC/LICS, IEMN, UMR CNRS 8520, Université Lille 1, Avenue Poincaré, 59652 Villeneuve d'Ascq, France. E-mail: michael.baudoin@univ-lille1.fr; farzam.zoueshtagh@univ-lille1.fr

† Electronic supplementary information (ESI) available. See DOI: 10.1039/c4sm01648c

‡ These authors contributed equally to this work.

Published on 11 September 2014. Downloaded by Univ Lille 1 on 05/02/2015 13:44:30.

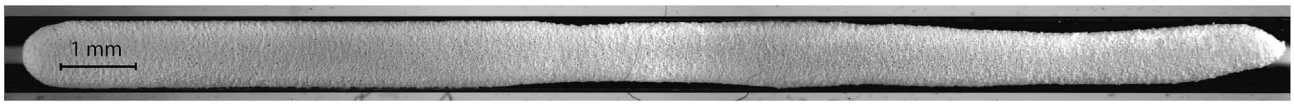

Fig. 1 Cylindrical armoured bubble covered with a monolayer of 15 μm polyamide particle surrounded by water inside a capillary tube of diameter 1 mm.

capillary tube of mean radius $R_w = 501$ μm covered with Rilsan (Polyamide 11) particles of mean radius $R_p = 15$ μm ± 1 μm (see Fig. 2). These particles were scattered in the tube prior to experiments by gently blowing them with an air jet. The dynamics of the moving meniscus is recorded with a CCD camera mounted on a microscope. To avoid diffraction of light by the cylindrical walls, the tube is trapped between two microscope slides and surrounded with an index-matching liquid.

Different wetting configurations were considered (i) by using liquids with different surface tensions (DI water, water/ethanol mixtures, perfluorodecalin) and (ii) by chemically treating the tubes walls to modify their surface energy.

2.2 Capillary tube treatment

Tubes inner walls were treated either with piranha solution (sulfuric acid + hydrogen peroxide), or with Self Assembled Monolayers (SAMs) (silanization process) of different organic molecules: perfluorodecyltrichlorosilane§ (PFTS) or hexamethyldisilazane¶ (HDMS). Piranha solution cleans the organic residues off the glass and leads to perfectly wettable glass walls. SAMs are molecular layers which modify the surface energy of the treated solid in a proportion which depends on the organic molecule adsorbed on the surface.[24,25] SAMs are classically used in labs on chips and droplet microfluidics to turn high energy surfaces such as glass or crystals into hydrophobic surfaces.[26–28]

Capillary tube cleaning. Glass capillaries were freshly cleaned and oxidized to provide a dense array of reactive silanol groups (≡SiOH), which are anchoring sites for the organosilane molecules. Capillaries were first degreased by sonication in dichloromethane, then isopropanol for 5 min. Glass substrates were perfectly dried under nitrogen flow, then in an air oven at 120 °C for 30 min. Then, the samples were dipped into a freshly prepared piranha solution (H_2SO_4, H_2O_2 2 : 1 v/v) at 100 °C for 15 min. They were rinsed thoroughly with deionized water, then were dried under nitrogen stream. To remove water inside capillaries, they were dried in an air oven at 120 °C for 1 h. This cleaning procedure was used to obtain perfectly wettable glass walls but also to prepare the tubes for their silanization. The drying procedure in the last step is very important for silanization since water excess is problematic as it causes hydrolysis and polymerization of organosilane molecules in solution.

Silanization‖. Glass capillaries were coated with SAMs using two organosilanes bearing either methyl (HDMS) or perfluorated (PFTS) functions. By a well-known mechanism (see Fig. 3), these molecules spontaneously react with the silanol ≡SiOH groups on the glass surface providing a hydrophobic molecular film. The silanization reactions were carried out in a glovebox under nitrogen atmosphere since HMDS and PFTS are water sensitive. The cleaned glass capillaries were immersed for 2 h in a 10^{-3} M solution of organosilane in a mixture of *n*-hexane and dichloromethane (70 : 30 v/v). Capillaries were cleaned thoroughly in dichloromethane (2 times) by sonication, then blown with dry nitrogen.

Wetting properties of the walls and particles. The wetting properties of the walls and particles for each surface treatment and liquid were characterized respectively by the static contact angles θ_w and θ_p for negative spreading parameters S_w and S_p. The spreading parameter gauges the ability of a liquid to wet a solid surface. When the spreading coefficient is positive, the liquid wets the surface completely. When it is negative, the liquid wets partially the solid surface and thus the gas interface meets the solid–liquid interface with an angle called the contact angle. The wetting properties of the walls for the different liquids used in our experiments (DI water, water/ethanol mixtures, perfluorodecalin) were measured by applying the

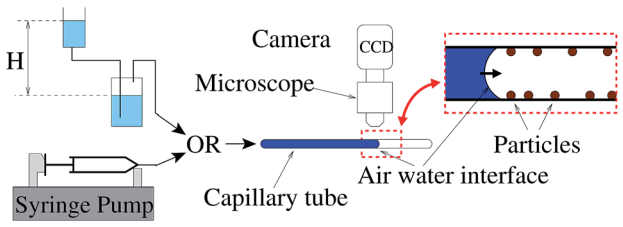

Fig. 2 Experimental setup.

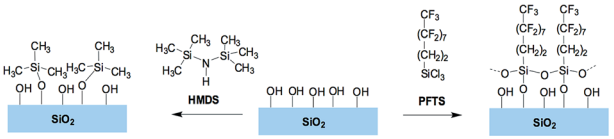

Fig. 3 Silanization process.

§ 1*H*,1*H*,2*H*, 2*H*-Perfluorodecyltrichlorosilane $CF_3(CF_2)_7(CH_2)_2SiCl_3$.

¶ Hexamethyldisilazane $(CH_3)_3SiNHSi(CH_3)_3$.

‖ HMDS and PFTS were obtained from Gelest. Dichloromethane (99.9%, amylene stabilized) was obtained from Scharlau. *n*-Hexane (99%, ACS grade) and isopropanol (99.7%) were purchased from Carlo Erba. Sulfuric acid (98%) and hydrogen peroxide (30% in water) were purchased from Sigma Aldrich. All chemicals were used as received without further purification. Deionized water (18 MΩ cm) was used to rinse substrates.

 This journal is © The Royal Society of Chemistry 2014

Published on 11 September 2014. Downloaded by Univ Lille 1 on 05/02/2015 13:44:30.

Table 1 Values of the static contact angle (when the spreading parameter S is negative) with the walls θ_w and particles θ_p for the different liquids used in the experiments and different walls chemical treatments. When the liquid fully wets the walls or the particles, the spreading parameter is positive

	Glass	Glass treated with HDMS	Glass treated with PFTS	Particles
DI water	$S_w > 0$	$\theta_w = 62 \pm 1$	$\theta_w = 106 \pm 8$	$\theta_p = 71 \pm 3$
Water-Eth. 6%	$S_w > 0$	$\theta_w = 62 \pm 1$	$\theta_w = 88 \pm 3$	$\theta_p = 71 \pm 5$
Water-Eth. 27%	$S_w > 0$	$\theta_w = 51 \pm 3$	$\theta_w = 80 \pm 1$	$\theta_p = 48 \pm 1$
Perfluorodecalin	$S_w > 0$	$\theta_w = 10 \pm 4$	$\theta_w = 34 \pm 3$	$S_p > 0$
Ethanol	$S_w > 0$	$S_w > 0$	$\theta_w = 42 \pm 4$	$S_p > 0$

same chemical treatment to a glass wafer as the one applied to the capillary tube and then measuring the static contact angle of a sessile droplet deposited on the substrate. The wetting properties of the particles were characterized by the same method after having coated the glass wafer with a thin film of Rilsan obtained by melting down the particles. These wetting properties are summarized in Table 1.**

3 Experimental results

3.1 Liquid finger pushed at constant flow rate

Experiments have been performed for all wetting configurations described in Table 1. In this section, the liquid is pushed at constant flow rate $Q = 3$ μl min^{-1}. We identified four main regimes with respect to the walls and particles wetting properties (see phase diagram in Fig. 4).

Regime 1. Perfectly wettable particles ($S_p > 0$). Here, particles are weakly affected by the motion of the meniscus for both cases of perfectly ($S_w > 0$) and partially ($S_w < 0$) wettable walls. For perfectly wettable walls ($S_w > 0$), a liquid film is present ahead of the meniscus due to local evaporation and condensation in front of the meniscus. In such a situation, the passage of the meniscus across the particles has no or negligible effect since the particles are already immersed in the liquid film prior to the meniscus arrival (Fig. 5A and Movie S1†). For partially wettable walls however ($S_w < 0$), there is no macroscopic liquid film ahead of the meniscus. As a consequence, particles are attracted by the liquid as soon as they are touched by the interface and then simply released behind the meniscus (Fig. 5B and Movie S2†).

Regime 2. Perfectly wettable walls ($S_w > 0$) and partially wettable particles ($S_p < 0$, $\theta_p \in [0,\pi/2]$). This regime leads to the formation of armoured bubbles. At the beginning, particles are collected at the surface of the meniscus until it becomes entirely covered with a monolayer of packed particles (see Fig. 6B, Movie S3†). Then, the interface keeps growing, through the development of a particle-covered liquid film ahead of the meniscus. This results in the formation of a long gas finger covered with particles (Fig. 6C, Movie S4†). This gas finger eventually collapses (see Fig. 6D, Movie S5†) and forms a long cylindrical armoured bubble (see *e.g.* Fig. 1).

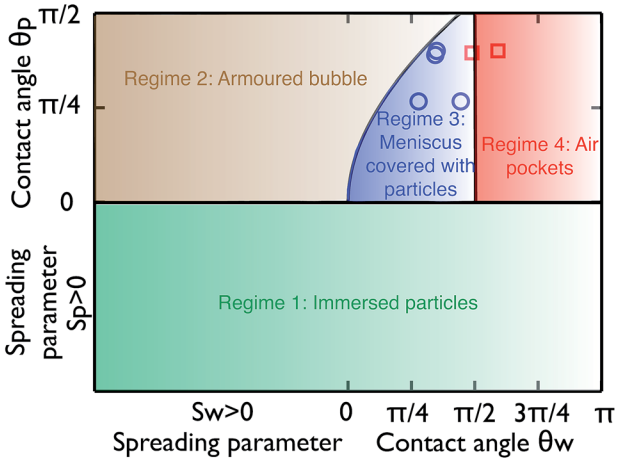

Fig. 4 Phase diagram summarizing the four regimes observed depending on the spreading parameters S_p and S_w of the walls and particles or the contact angles θ_p and θ_w when the spreading parameter is negative. The line separating regimes 2 and 3 has been computed according to eqn (5). Since the values of the spreading parameters is not known when it is positive for the material used in our experiments, only data with $S_p < 0$ and $S_w < 0$ are represented in this graph.

Regime 3. Walls with high wettability ($S_w < 0$, $\theta_w < \pi/2$) and partially wettable particles ($S_p < 0$) with $\theta_p \in [0, \theta_c]$.†† Particles are first collected at the surface of the meniscus until it becomes entirely covered with a monolayer of packed particles (see Fig. 7B), similarly to Regime 2. Then, new particles contribute to the growth of the particle-covered interface through a reduction of the apparent contact angle with the surface down to a limiting value, θ_l. Once this limiting value is reached, new particles which come into contact with the meniscus are immersed inside the liquid finger (see Fig. 7C and Movie S3†).

** The exact value of the spreading parameter when the liquid wets the surface completely ($S > 0$) is difficult to determine since it requires the knowledge of the solid–gas and solid–liquid surface energies. When it is negative however, it is linked to the contact angle θ and the surface tension γ_{GL} according to the formula: $S = \gamma_{GL}(\cos\theta - 1)$.

†† θ_c is the critical contact angle defined by eqn (5).

Published on 11 September 2014. Downloaded by Univ Lille 1 on 05/02/2015 13:44:30.

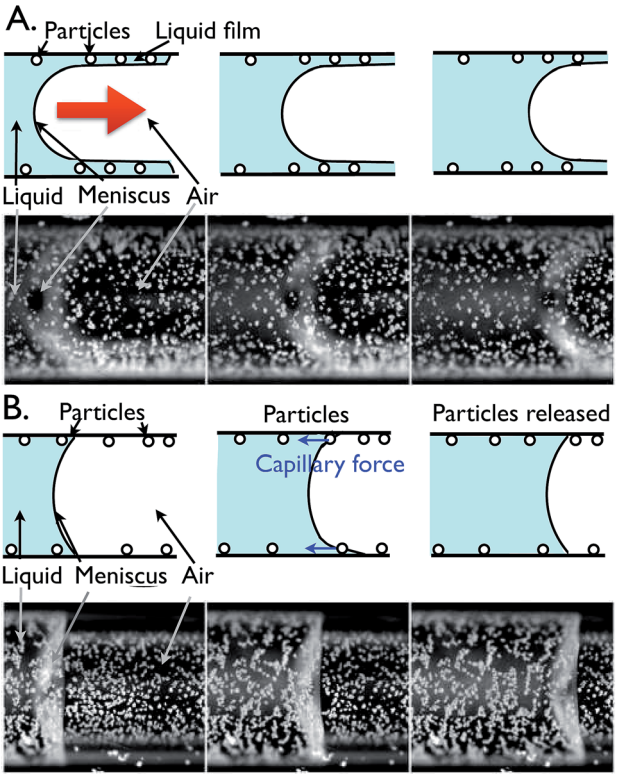

Fig. 5 Regime 1: Schematic and snapshots of experiments showing the evolution of a liquid finger pushed at constant flow rate inside a capillary tube covered with perfectly wettable particles (white dots in the pictures). (A) Perfectly wettable walls (B). Partially wettable walls.

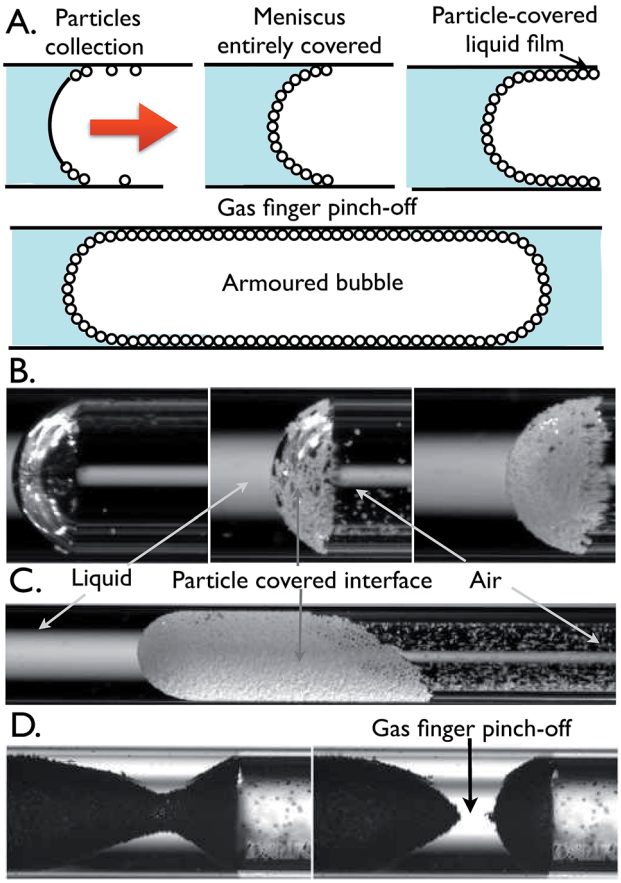

Fig. 6 Regime 2: Liquid finger pushed at constant flow rate inside a perfectly wettable capillary tube covered with partially wettable particles. (A) Schematic of the evolution of the air–liquid interface. (B) Particles are collected until they cover the whole meniscus. (C) A liquid layer covered with a monolayer of particles grows ahead of the meniscus leading to the formation of an encapsulated gas finger. (D) The pinch-off of the gas finger results in the formation of an armoured bubble (Fig. 1). Particles appear in dark in picture D since the lighting conditions were different.

Regime 4. Walls with low wettability ($S_w < 0$, $\theta_w > \pi/2$) and partially wettable particles ($S_p < 0$). In this case, the particles accumulate along the contact line and obstruct its motion. Since the flow rate is imposed, the meniscus eventually bypasses the particles. This gives rise to the formation of air pockets trapped between the tube's wall and the liquid inside the capillary, and whose surface is covered with particles (see Fig. 8 and Movie S7†).

3.2 Liquid finger pushed at constant pressure

Further experiments were conducted in regime 2 to determine the evolution of the encapsulated bubbly finger resistance to motion and gain physical insight of the reason for its collapse into and armoured bubble. In these experiments a long liquid plug is pushed at constant pressure head $\Delta P = 0.2$ kPa inside a perfectly wettable capillary tube covered with Rilsan particles (see Fig. 9A and B and Movies S8 and S9†). In the absence of particles, experiments in the literature[29] indicate that a plug pushed at constant pressure experiences a gradual increase of its velocity due to a progressive decrease of its resistance to motion. Instead, in the present experiment, a gradual decrease in the plug's velocity is observed along with a stick-slip motion of the plug when the length of the encapsulated finger becomes sufficiently large (see Fig. 9C).

4 Discussion and theoretical modeling

In this section, the different regimes observed experimentally are discussed and simple energetic considerations are developed to provide basic understanding of the observed tendencies.‡‡ In all the experiments described above, the Reynolds number $\mathrm{Re} = \rho_l U R_w/\mu_l$, Capillary number $\mathrm{Ca} = \mu_l U/\gamma_{GL}$ and Bond number $\mathrm{Bo} = \rho_l g {R_w}^2/\gamma_{GL}$ remain small:

$$\mathrm{Re} \lesssim 10^{-2}, \mathrm{Bo} \lesssim 10^{-1} \text{ and } \mathrm{Ca} \lesssim 10^{-6}$$

‡‡ As a first approximation, particles are supposed to be perfectly spherical in the following calculations while this is not the case experimentally. Higher order effects could therefore appear in this case such as particle–particle interaction due to the asymmetry of the particles. Nevertheless, they would not fundamentally modify the liquid film deposition mechanism proposed here.

This journal is © The Royal Society of Chemistry 2014

Published on 11 September 2014. Downloaded by Univ Lille 1 on 05/02/2015 13:44:30.

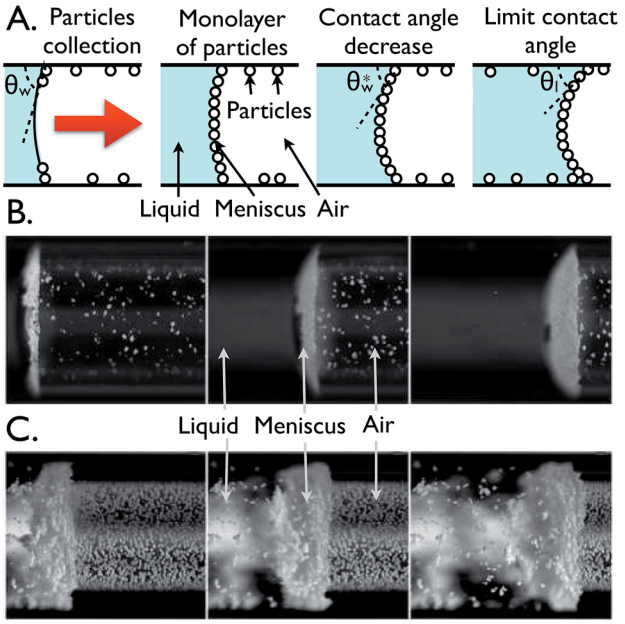

Fig. 7 Regime 3: Liquid finger pushed at constant flow rate inside capillary tubes with highly wettable walls covered with partially wettable particles whose contact angle θ_p is under the critical value θ_c defined by eqn (5). (A) Schematic illustrating the evolution of the meniscus. (B) Snapshots of the capillary tube showing the collection of the particles encountered by the meniscus and the reduction of the contact angle. (C) Evolution of the meniscus once the contact angle has reached a limiting value θ_l.

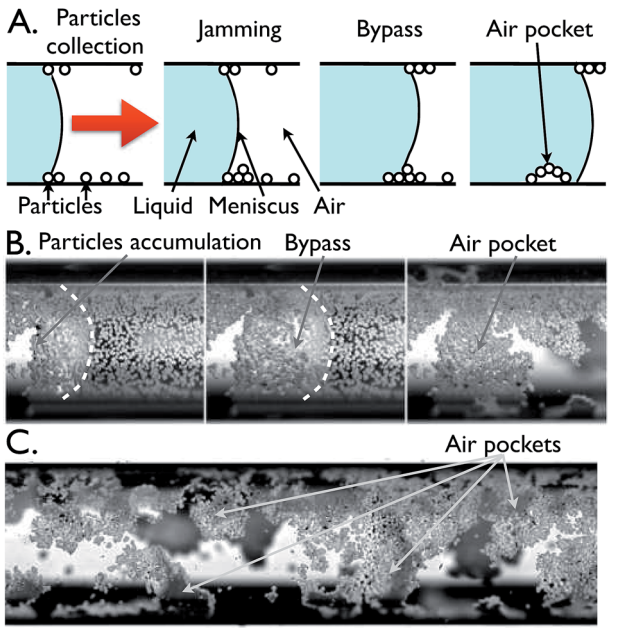

Fig. 8 Regime 4: Liquid finger pushed at constant flow rate inside a capillary tube with low wettability covered with partially wettable particles. (A) Schematic illustrating the evolution of the meniscus. (B) Snapshots showing the formation of an air pocket. The dashed white line indicates the position of the meniscus. (C). Final state after the passage of the meniscus.

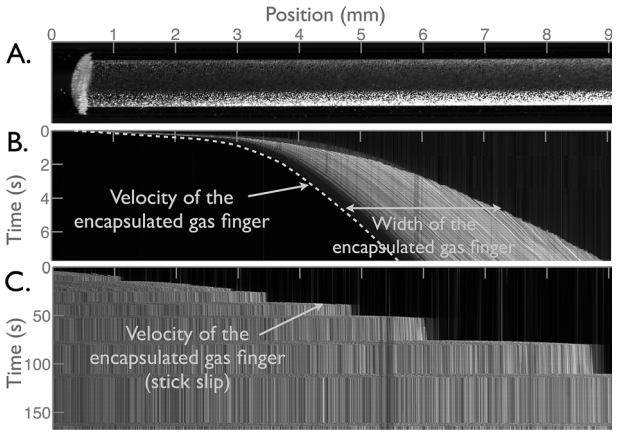

Fig. 9 Evolution of a liquid plug pushed at constant pressure in a wetting tube covered with partially wettable particles. (A) Initial configuration: the front meniscus is covered with a monolayer of particles. (B) Spatiotemporal diagram displaying the grey values along the center line of the channel as a function of time. Velocities and lengths of the encapsulated gas finger are respectively obtained from the slopes of the boundaries of the grey part of the graph and the distance between them. The grey dashed line delimit the left part of the bubble. (C) Spatiotemporal diagram showing the evolution of the right part of the encapsulated gas finger when its length is equal to 1.6 cm. The velocity of the gas-finger is given by the boundary between the grey part (particles) and the dark one (liquid). The steps indicate stick-slip motion.

with ρ_l, μ_l and γ_{GL}, the density, viscosity and surface tension of the considered liquid respectively, $U = Q/(\pi R_w^2)$, the characteristic velocity of the liquid finger and g the gravitational acceleration.§§ This means that, away from the contact line (where the triple line introduces a flow singularity), surface tension effects are dominant over those of inertia, gravitation and viscosity. The shape of the meniscus is therefore only determined by the minimization of surface energy. Furthermore, since the capillary number is extremely small, the dynamic contact angle differs only slightly from the static contact angle¶¶ and thus, the evolution of the meniscus can be considered as quasi-static (that is to say a succession of equilibrium states).

When the first particles come into contact with the meniscus, the system spontaneously selects the configuration which minimizes the total interfacial energy E. The latter is the sum of the gas–liquid (GL), gas–wall (GW), liquid–wall (LW), gas–particle (GP) and liquid-particle (LP) energy:

$$E = \gamma_{GL}A_{GL} + \gamma_{GW}A_{GW} + \gamma_{LW}A_{LW} + \gamma_{GP}A_{GP} + \gamma_{LP}A_{LP}$$

§§ In regime 2, the characteristic velocity of the liquid film is of the same order of magnitude as the velocity U. Indeed, the liquid film velocity is equal to the sum of the meniscus velocity and the expansion velocity of the liquid film. The latter depends on the concentration of particles on the walls prior to the experiment. In the experiments performed here, the characteristic velocity of the liquid film is typically 15% higher than the velocity of the meniscus and thus does not modify the estimation of the capillary number provided in this section.

¶¶ Hoffman–Tanner law[22,23] predicts a dynamic contact angle $\leq 3°$ for a perfectly wetting liquid moving at a capillary number Ca $\sim 10^{-6}$.

Published on 11 September 2014. Downloaded by Univ Lille 1 on 05/02/2015 13:44:30.

where γ and A are the tension and area of the corresponding interface, respectively. The global constraint of minimum energy leads to 3 local constraints: (i) the liquid–gas interface satisfies Young–Laplace's equation and adopts a spherical shape, and the triple lines (ii) on the wall and (iii) at the particle surface satisfy Young–Dupré's equation:

$$\cos\theta_w = \frac{\gamma_{GW} - \gamma_{LW}}{\gamma_{GL}}, \quad \cos\theta_p = \frac{\gamma_{GP} - \gamma_{LP}}{\gamma_{GL}} \tag{1}$$

with θ_w and θ_p, the wall and particle static contact angles, respectively. As a result of condition (iii), perfectly wettable particles ($S_p > 0$) are immersed in the liquid (regime 1) whereas partially wettable particles ($S_p < 0$) are trapped at the interface (regime 2, 3 and 4). For wettable walls ($\theta_w < \pi/2$, regimes 2 and 3), the same condition applies for the successive particles until the meniscus is entirely covered with a monolayer of particles. For walls with low wettability ($\theta_w > \pi/2$) however (regime 4), particles captured at the contact line prevent the liquid from coming into contact with new particles due to jamming (see Fig. 8A) and so, the lowest energy state cannot be reached. Particles accumulate along the contact line and obstruct its motion. As the flow rate is imposed, the liquid finger is pushed forward and the contact line eventually bypasses the pile of particles resulting in the formation of air pockets on the tube's wall (see Fig. 8C).

We will now discuss regimes 3 once the meniscus is entirely covered with a monolayer of particles. When new particles come into contact with the meniscus, three different situations can occur: (i) particles are immersed in the liquid phase, (ii) they are integrated into an extended meniscus, or (iii) they stay in the gas phase. Since in regimes 2 and 3 the particles are partially wettable, interfacial energy is always lower in configuration (ii) as compared to (iii). Thus, situation (iii) cannot occur in the absence of additional constraints.

Now the following calculations are aimed at forecasting the system selection between configurations (i) and (ii) by determining the least energetic configuration according to values of contact angles θ_w and θ_p. To calculate the energy difference δE between configurations (i) and (ii), one can determine the energy required for the transition between these two states.

This transition can be decomposed into two steps (see Fig. 10): (1) the surface of the meniscus increases to leave enough space to integrate a new particle (variation of energy δE^+) and (2) the particle migrates at the air–liquid interface (variation of energy δE^-):

$$\delta E = \delta E^+ + \delta E^- \tag{2}$$

In configuration (ii), the absorption of a new particle by the meniscus requires the expansion of its surface by $\delta S = \pi {R_p}^2/\phi$, where ϕ is the specific surface area as defined by Torquato[30] ($\phi \approx 0.8$ for spheres in a 2D configuration). Indeed due to their shape, the particles occupy only a fraction of the air–liquid interface. For partially wettable walls, this expansion leads to a decrease of the contact angle by $\delta\theta_w^* = [\cos^3(\theta_w)/(2(\sin(\theta_w^*)(2 - \sin(\theta_w^*)) - 1))][R_p^2/(R_w^2\phi)]$, which in turn yields an increase in interfacial energy by:

$$\delta E^+ = \frac{\pi\gamma_{GL}{R_p}^2}{\phi}\left[1 - \frac{\cos(\theta_w)}{\cos(\theta_w^*)}\right]$$

where θ_w^* is the apparent contact angle sustained by the presence of particles at the interface (see Appendix A for details of this calculation). On the other hand, the integration of a new particle to the interface leads to a decrease of interfacial energy by:

$$\delta E^- = -\gamma_{GL}\pi{R_p}^2[1 - \cos(\theta_p)]^2$$

since a partially wettable particle lies in its less energetic configuration when it is trapped at an air–liquid interface with a contact angle θ_p. Thus, configuration (ii) is energetically favorable if:

$$\delta E = \pi\gamma_{GL}{R_p}^2\left[\frac{1}{\phi}\left(1 - \frac{\cos(\theta_w)}{\cos(\theta_w^*)}\right) - (1 - \cos(\theta_p))^2\right] < 0. \tag{3}$$

This function is always negative at the beginning when $\theta_w^* = \theta_w$ and results in a decrease in the apparent contact angle θ_w^* until it reaches a limit value θ_l corresponding to $\delta E = 0$:

$$\cos(\theta_l) = F(\theta_p,\theta_w) = \frac{\cos(\theta_w)}{1 - \phi(1 - \cos(\theta_p))^2}. \tag{4}$$

Then, new incoming particles are immersed into the liquid phase (regime 3). However, if $F(\theta_p,\theta_w) \geq 1$, that is to say:

$$\theta_p \geq \theta_c = a\cos\left[1 - \sqrt{\frac{1 - \cos(\theta_w)}{\phi}}\right] \tag{5}$$

Eqn (4) has no solution and thus the contact angle decreases down to 0. At this stage, the interface can only expand ahead of the meniscus with the development of a liquid film which recovers the wall (regime 2). Calculations (see Appendix B) indeed show that this liquid expansion is energetically

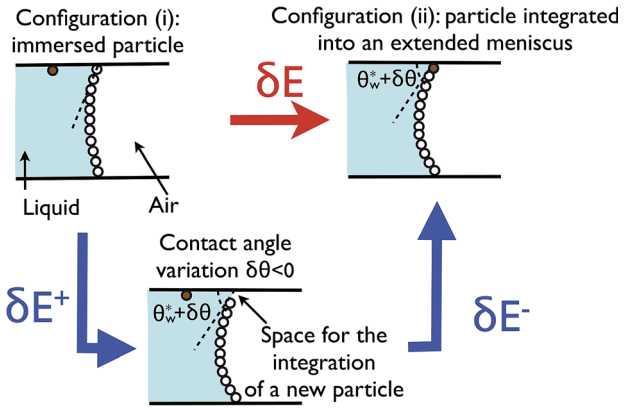

Fig. 10 Transition between configuration (i) and (ii).

This journal is © The Royal Society of Chemistry 2014

Published on 11 September 2014. Downloaded by Univ Lille 1 on 05/02/2015 13:44:30.

favorable when criterion (5) is verified or when the walls are perfectly wetting ($S_w > 0$) and the particles partially wetting ($S_p < 0$). This minimization of the surface energy thus explains the growth of the particle-covered interface through the deposition of a film ahead of the meniscus observed in regime 2.

This liquid film is stabilized by particles jamming in the monolayer, which prevents the development of Rayleigh-Plateau instability. The air finger pinch-off is only enabled by the large pressure head increase resulting from the increase in the resistance of the encapsulated finger to motion. Indeed, the motion of liquid plugs and fingers in micro-channels can be described through an Ohm-like law, $\Delta P = Qr_b$, where ΔP is the pressure drop along the channel and r_b is the liquid plug's or finger's resistance to motion.[29] In Section 3.2, experiments performed at constant pressure indicate a drastic reduction of the velocity of the encapsulated bubbly finger when its size increases through the collection of particles lying on the walls. This reduction of the velocity indicate an increase in the resistance r_b. At constant flow rate, this resistance increase will lead to a large increase in the driving pressure head, which eventually provokes the pinch-off of the gas finger. The prediction of the final size of the armored bubble would require the knowledge of (i) the pressure required for the pinch-off of the bubble and (ii) the evolution of the pressure head resulting from the increase of the bubble resistance to motion. This increase of resistance might have different origins such as the friction of particles with the walls or the viscous dissipation in the liquid film separating the bubble from the tube. Further experiments would be required to determine the comparative contributions of these phenomena.

5 Conclusion and perspectives

In this paper, we study the strongly modified dynamics of a liquid finger pushed inside a capillary tube when particles are lying on the walls. Different regimes are observed according to the wetting configuration. One of these regimes leads to the controlled formation of armoured bubbles covered with a monolayer of particles, whose shape and lateral size is prescribed by the geometry of the capillary tube. This system enables a serial production of such armoured bubbles. Indeed, once an armoured bubbles is formed another starts growing in the remaining part of the tube, and so on until all the particles lying on the walls have been collected. These encapsulated bubbles can then be extracted from the capillary tube by pushing them with a higher flow rate. Once out of the tube, they keep their cylindrical shape since the jamming of particles prevents the reduction of the bubble surface (see Fig. 11). This works opens perspectives for low cost automatic production of armoured bubbles with specific geometries. The production of a large number of identical armoured bubbles would nevertheless require a parallelization and an optimization of the present experimental setup to obtain bubbles with predictable lengths.

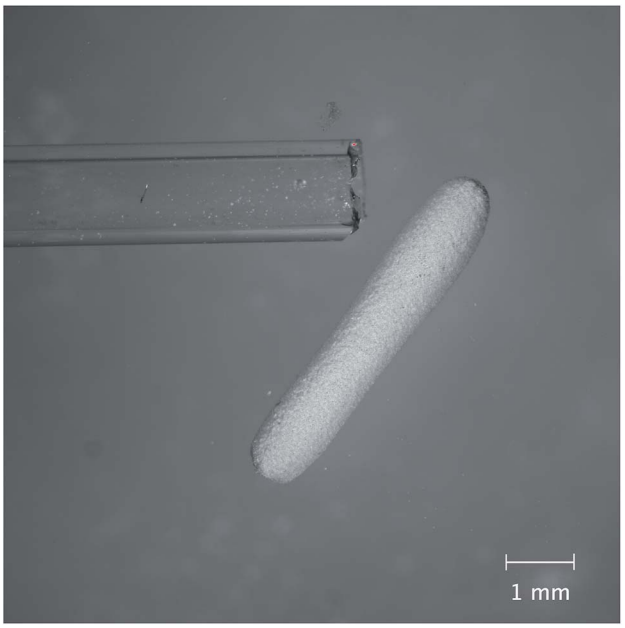

Fig. 11 Stable cylindrical armoured bubble extracted from the tube. It is obtained by pushing the long armored bubble formed in the capillary tube with a higher flow rate into a larger cell. In these preliminary experiments, the buoyancy force resulted in the division of the long armored bubble into smaller bubbles.

The present method might, in principle, be extended to the production of encapsulated bubbles in a colloidal crystal[31,32] or ordered two dimensional arrays[33] if neutral particles are replaced by strongly interacting ones. For macroscopic particles, these interactions can result from the balance of gravity and surface tension, the so-called "Cheerios" effect.[34,35] At smaller scales (micrometer to nanometer range), gravity is negligible and so interaction can be induced by electrical charges,[31,36] irregular shape,[37] roughness,[38] or inhomogeneous wetting properties of the particles.[33] They could also be triggered by interface curvature as demonstrated recently by Würger.[39]

These singular bubbles are interesting for their static properties (stability, original shape); but their strongly nonlinear dynamics also opens new perspective for the design of original acoustical materials such as contrast agents.

Appendix A: decrease of the apparent contact angle induced by the presence of particles on the walls

This appendix is giving the details of calculations for the variations of energy, $\delta E = \delta E^{+} + \delta E^{-}$ expressed in eqn (3). Here, we will only consider particles with small radius R_p compared to the radius of curvature of the meniscus R_c and thus neglect the interface curvature at the scale of a particle. This hypothesis is well verified in our experiments since $R_p/R_c < 2 \times 10^{-2}$. We will also suppose that the evolution is quasi-static, as justified in the main text.

Published on 11 September 2014. Downloaded by Univ Lille 1 on 05/02/2015 13:44:30.

Increase of energy due to the decrease of the contact angle

In absence of particles, the contact angle at the liquid–air–wall triple line is given at rest by Young–Dupré's equation:

$$\cos\theta_w = \frac{\gamma_{GW} - \gamma_{LW}}{\gamma_{GL}} \quad (6)$$

where γ_{GW}, γ_{LW} and γ_{GL} are the gas–wall, liquid–wall and gas–liquid tensions respectively. This equation can be simply deduced from a minimization of the interfacial energy. The integration of an additional particle to the air–liquid interface requires an increase of the meniscus surface δA_{GL} through a reduction of the contact angle $\delta\theta_w^*$. This surface increase, δA_{GL}, yields to an increase of interfacial energy $\delta E^+ = dE_w/d\theta_w^* \delta\theta_w^*$ where $E_w = \gamma_{GL}A_{GL} + \gamma_{GW}A_{GW} + \gamma_{LW}A_{LW}$ is the sum of the gas–liquid, gas–wall and liquid–wall interfacial energy in absence of particles and θ_w^* is the wall apparent contact angle at a certain point of the evolution. We must therefore determine the expressions of $\delta\theta_w^*$ and $E_w(\theta_w^*)$ to estimate δE^+.

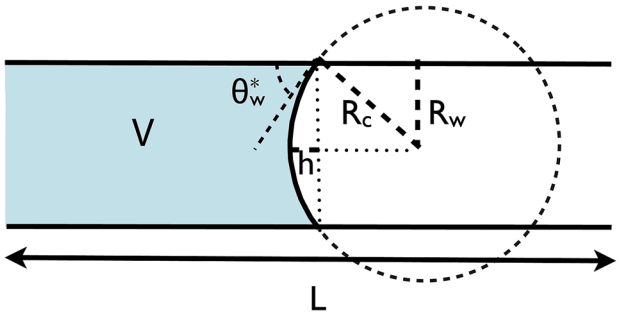

Fig. 12 Schematic of the meniscus.

Computation of $\delta\theta_w^*$. Due to their shape and arrangement, the particles cover only a fraction, ϕ, of the air–liquid interface, called the specific surface area. The air–liquid surface increase δA_{GL} required for the integration of a single particle is therefore:

$$\delta A_{GL} = \pi R_p^2/\phi. \quad (7)$$

Suppose that the wall apparent contact angle at a certain point of the evolution is equal to θ_w^* (with $\theta_w^* = \theta_w$ just prior to meniscus surface increase, *i.e.* when the first additional particle reaches the meniscus which has its surface fully covered by particles). The surface of the meniscus A_{GL} can be expressed as a function of θ_w^* according to (see Fig. 12):

$$A_{GL} = 2\pi R_c h = 2\pi R_c \times (1 - \sin(\theta_w^*))R_c \quad (8)$$

$$= \frac{2\pi R_w^2(1-\sin\theta_w^*)}{\cos^2\theta_w^*} \quad (9)$$

with $R_c = R_w/\cos(\theta_w^*)$ the radius of curvature of the meniscus, R_w the tube radius and h the height of the meniscus. From this formula, we can compute the decrease of contact angle $\delta\theta_w^*$ resulting from the increase of interface δA_{GL}:

$$A_{GL} + \delta A_{GL} = \frac{2\pi R_w^2(1-\sin(\theta_w^* + \delta\theta_w^*))}{\cos^2(\theta_w^* + \delta\theta_w^*)} \quad (10)$$

Since $\delta A_{GL} \ll A_{GL}$ and $\delta\theta_w^* \ll \theta_w^*$, the first order taylor series expansion gives:

$$\delta A_{GL} = [\sin\theta_w^*(2 - \sin\theta_w^*) - 1]\frac{2\pi R_w^2}{\cos^3\theta_w}\delta\theta_w^* \quad (11)$$

Finally the combination of eqn (7) and (11) gives:

$$\delta\theta_w^* = \frac{\cos^3\theta_w^*}{2[2\sin\theta_w^* - \sin^2\theta_w^* - 1]}\frac{R_p^2}{R_w^2\phi} \quad (12)$$

Computation of $E_w(\theta_w^*)$ and its derivative. To compute, the relation between the interfacial energy E_w and the contact angle θ_w^*, we will consider a cylindrical capillary tube of length L and radius R_w partially filled with a volume V of liquid and a volume $\pi R_w^2 L - V$ of gas (see Fig. 12). The interfacial energy E_w is given by:

$$E_w = \gamma_{GL}A_{GL} + \gamma_{GW}A_{GW} + \gamma_{LW}A_{LW}$$

with the interfacial areas A_{LW} and A_{GW} given by:

$$A_{LW} = 2\pi R_w\left[\frac{V}{\pi R_w^2} + \frac{R_w}{3\cos^3\theta_w^*}(1-\sin\theta_w^*)^2(\sin\theta_w^* + 2)\right] \quad (13)$$

$$A_{GW} = 2\pi R_w L - A_{LW} \quad (14)$$

Expression of δE^+. Combination of eqn (7), (12), (13) and (14) gives:

$$\delta E^+ = \frac{dE_w}{d\theta_w^*}\delta\theta_w^* = \frac{d(\gamma_{GW}A_{GW} + \gamma_{LW}A_{LW})}{d\theta_w^*}\delta\theta_w^* + \gamma_{GL}\delta A_{GL}$$
$$= \left[\frac{2\pi R_w^2(\gamma_{GW} - \gamma_{LW})}{2\sin\theta_w^* + (\sin^2\theta_w^* + 1)}\right]$$
$$\times\left[\frac{\cos^3\theta_w^*}{2[2\sin\theta_w^* - (\sin^2\theta_w^* + 1)]}\frac{R_p^2}{R_w^2\phi}\right] + \frac{\gamma_{GL}\pi R_p^2}{\phi} \quad (15)$$

Since $\gamma_{GW} - \gamma_{LW} = \gamma_{GL}\cos\theta_w$ and $[1 - 2\sin^2\theta_w^* + \sin^4\theta_w^*] = \cos^4\theta_w^*$, eqn (15) can be simplified into:

$$\delta E^+ = \frac{\gamma_{GL}\pi R_p^2}{\phi}\left[1 - \frac{\cos\theta_w}{\cos\theta_w^*}\right] \quad (16)$$

In regimes 2 and 3, walls are respectively perfectly and highly wettable ($0 \le \theta_w^* \le \theta_w < \pi/2$) and, as expected, δE^+ is positive.

Decrease of energy due to the integration of a particle at the meniscus

When a particle comes into contact with an air–liquid interface, the system adopts the minimal energy configuration, in absence of additional constraint. A partially wettable particle will therefore be trapped at the air–liquid interface with an angle given by Young Dupré's equation around the particle:

$$\cos\theta_p = \frac{\gamma_{GP} - \gamma_{LP}}{\gamma_{GL}} \quad (17)$$

This journal is © The Royal Society of Chemistry 2014

Published on 11 September 2014. Downloaded by Univ Lille 1 on 05/02/2015 13:44:30.

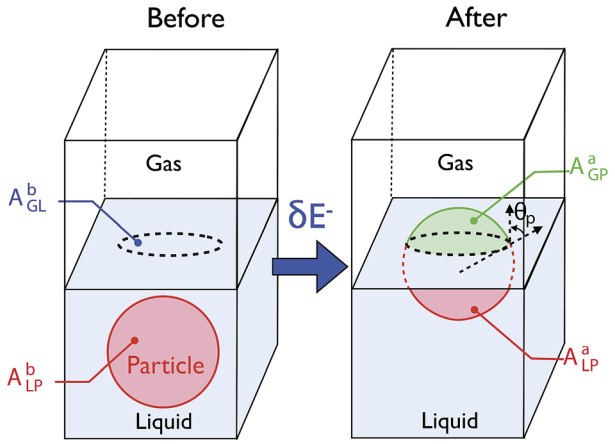

Fig. 13 Migration of a particle to the meniscus.

Therefore, the migration of a particle from the liquid phase to the interface corresponds to a decrease of the interfacial energy δE^-. This variation can be computed by subtracting the interfacial energy before and after the migration of the particle (see Fig. 13):

$$\delta E^- = [\gamma_{GP}A^a_{GP} + \gamma_{LP}A^a_{LP}] - [\gamma_{GL}A^b_{GL} + \gamma_{LP}A^b_{LP}] \quad (18)$$

From Fig. 13, we easily obtain.

$$\delta E^- = \gamma_{GP}[2\pi R_p{}^2(1 - \cos(\theta_p))] + \gamma_{LP}[2\pi R_p{}^2(1 + \cos\theta_p)] - \gamma_{GL}[\pi R_p{}^2 \sin^2\theta_p] - \gamma_{LP}[4\pi R_p{}^2] \quad (19)$$

Combining eqn (17) and (19), we obtain:

$$\delta E^- = -\gamma_{GL}\pi R_p{}^2[1 - \cos\theta_p]^2 \quad (20)$$

This expression is effectively always negative whatever the value of the contact angle θ_p.

Expression of δE

The difference of interfacial energy between configurations (i) and (ii) is now simply obtained by replacing expressions (16) and (20) into eqn (2):

$$\delta E = \delta E^+ + \delta E^- = \gamma_{GL}\pi R_p{}^2\left[\frac{1}{\phi}\left(1 - \frac{\cos\theta_w}{\cos\theta_w^*}\right) - (1 - \cos\theta_p)^2\right] \quad (21)$$

This function is always negative at the beginning when $\theta_w^* = \theta_w$. The minimization of interfacial energy therefore induces the integration of new particles to the interface through a decrease of the apparent contact angle θ_w^* until it reaches a limit value θ_l corresponding to $\delta E = 0$:

$$\cos(\theta_l) = F(\theta_p, \theta_w) = \frac{\cos(\theta_w)}{1 - \phi(1 - \cos(\theta_p))^2}. \quad (22)$$

From then, next particles met by the meniscus enter the liquid phase (regime 3). However, since eqn (4) has a solution only if $F(\theta_p, \theta_w) \leq 1$, that is to say:

$$\theta_p \leq \theta_c = a\cos\left[1 - \sqrt{\frac{1 - \cos(\theta_w)}{\phi}}\right], \quad (23)$$

the contact angle will decrease down to 0 when $\theta_p \geq \theta_c$ (regime 2). Then, the interface can only expand ahead of the meniscus through the development of a liquid film which recovers the walls.

Appendix B: expansion of the interface through the deposition of a liquid film ahead of the meniscus (regime 2)

In this section, we will determine whether the expansion of the air–liquid interface ahead of the meniscus for the integration of new particles is energetically favorable. We therefore have to compare "configuration (a)" where the particle is immersed in the liquid phase and "configuration (b)" where it is incorporated into an extended air–liquid interface. The difference of interfacial energy between these two configurations $\delta E' = E^b - E^a$ can be simply calculated through careful comparison of these two states (see Fig. 14):

$$\begin{aligned}\delta E' = &\left[2\pi R_p{}^2(1 - \cos\theta_p)\gamma_{GP} + \pi R_p{}^2\left(\frac{1}{\phi} - \sin^2(\theta_p)\gamma_{GL}\right)\right. \\ &\left. + 2\pi R_p{}^2(1 + \cos\theta_p) + \frac{\pi R_p{}^2}{\phi}\gamma_{LW}\right] - \left[4\pi R_p{}^2\gamma_{LP}\right. \\ &\left. + \frac{\pi R_p{}^2}{\phi}\gamma_{GW}\right] \\ = &\left[2(1 - \cos\theta_p)(\gamma_{GP} - \gamma_{LP}) + \sin^2\theta_p\gamma_{GL}\right] \\ &- \frac{\pi R_p{}^2}{\phi}[\gamma_{GW} - (\gamma_{LW} + \gamma_{GL})] \end{aligned} \quad (24)$$

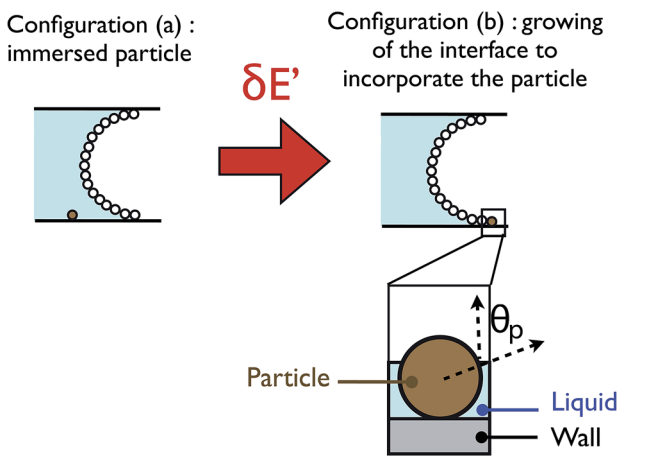

Fig. 14 Expansion of the meniscus.

Published on 11 September 2014. Downloaded by Univ Lille 1 on 05/02/2015 13:44:30.

By combining eqn (6), (17) and (24), one obtains:

$$\delta E' = \gamma_{GL}\pi {R_p}^2\left[-\frac{1}{\phi}S_w - \left(1-\cos\theta_p\right)^2\right] \quad (25)$$

$$= \gamma_{GL}\pi {R_p}^2\left[\frac{1}{\phi}(1-\cos\theta_w) - \left(1-\cos\theta_p\right)^2\right] \quad (26)$$

Note that this expression could have been obtained directly from previous calculation since it is a particular case of eqn (21) when $\theta_w^* = 0$:

$$\delta E' = \delta E(\theta_w^* = 0).$$

Careful examination of eqn (25) and (26) shows that $\delta E'$ is always negative when the walls are perfectly wettable ($S_w > 0$) or when the walls are partially wettable ($S_w < 0$) and $\theta_p \geq \theta_c$, with the expression of θ_c given in eqn (5). Thus in these two cases (corresponding to regime 2) the air–liquid interface covered with particles will expand through the deposition of a liquid film ahead of the meniscus.

Acknowledgements

The authors would like to thank Dr P. Brunet, Dr S. Giordano, Dr M. Gizolme and Dr S. V. Diwakar for their careful reading of the manuscript.

References

1 W. Ramsden, *Proc. R. Soc. London*, 1903, **72**, 156–164.
2 B. Johnson and R. Cooke, *Science*, 1981, **213**, 209–211.
3 B. Binks, *Curr. Opin. Colloid Interface Sci.*, 2002, **7**, 21–41.
4 B. P. Binks and T. S. Horozov, *Angew. Chem.*, 2005, 3722–3725.
5 J. Leja, *Surface chemistry of froth flotation*, Plenum Press, N.Y., 1982.
6 A. Dinsmore, M. Hsu, M. Nikolaides, M. Marquez, A. Bausch and D. Weitz, *Science*, 2002, **298**, 1006–1009.
7 B. Gibbs, S. Kermasha, I. Alli and C. Mulligan, *Int. J. Food. Sci. Nutr.*, 1999, **50**, 213–224.
8 F. Burmeister, W. Badowsky, T. Braun, S. Wieprich, J. Boneberg and P. Leiderer, *Appl. Surf. Sci.*, 1998, **461**, 144–145.
9 A. Subramaniam, M. Ankarian, L. Mahadevan and H. Stone, *Langmuir*, 2006, 10204–10208.
10 D. Vella, P. Aussillous and L. Mahadevan, *Europhys. Lett.*, 2004, **68**, 212–218.
11 D. Vella, H.-Y. Kim, P. Aussillous and L. Mahadevan, *Phys. Rev. Lett.*, 2006, **96**, 178301.
12 P. Aussillous and D. Quéré, *Nature*, 2001, **411**, 924–927.
13 C. Planchette, A.-L. Biance, O. Pitois and E. Lorenceau, *Phys. Fluids*, 2013, **25**, 042104.
14 A. Subramanian, M. Abkarian, L. Mahadevan and H. Stone, *Nature*, 2005, **438**, 930.
15 M. Abkarian, A. Subramaniam, S.-H. Kim, R. Larsen, S.-M. Yang and H. Stone, *Phys. Rev. Lett.*, 2007, **99**, 188301.
16 A. Subramaniam, M. Abkarian and H. Stone, *Nat. Mater.*, 2005, **4**, 553–556.
17 J. Park, Z. Nie, A. Kumachev, A. Abdelrahman, B. Binks, H. Stone and E. Kumacheva, *Angew. Chem., Int. Ed.*, 2009, **48**, 5300–5304.
18 W. Drencklan, *Angew. Chem., Int. Ed.*, 2009, **48**, 5245–5247.
19 M. Lee, V. Prasad and D. Lee, *Langmuir*, 2010, 2227–2230.
20 E. Tumarkin, J. Park, Z. Nie and E. Kumacheva, *Chem. Commun.*, 2011, 12712–12714.
21 F. Bretherton, *J. Fluid Mech.*, 1961, **10**, 166–188.
22 R. Hoffman, *J. Colloid Interface Sci.*, 1975, **50**, 228–241.
23 L. Tanner, *J. Phys. D: Appl. Phys.*, 1979, **12**, 1473.
24 A. Ulman, *Chem. Rev.*, 1996, **96**, 1533–1554.
25 R. Schreiber, *Prog. Surf. Sci.*, 2000, **65**, 151–256.
26 N. Glass, R. Tjeung, P. Chan, L. Yeo and J. Friend, *Biomicrofluidics*, 2011, 036501.
27 Z. Gurard-Levin and M. Mrksich, *Annu. Rev. Anal. Chem.*, 2008, **1**, 767–800.
28 M. Baudoin, P. Brunet, O. Matar and E. Herth, *Appl. Phys. Lett.*, 2012, **100**, 154102.
29 M. Baudoin, Y. Song, P. Manneville and C. Baroud, *Proc. Natl. Acad. Sci. U. S. A.*, 2013, **110**, 859–864.
30 S. Torquato, *Phys. Rev. E: Stat. Phys., Plasmas, Fluids, Relat. Interdiscip. Top.*, 1995, **51**, 3170–3182.
31 P. Pieranski, *Phys. Rev. Lett.*, 1980, **45**, 569–572.
32 W. Irvine, *Nature*, 2010, **468**, 947–950.
33 N. Bowden, A. Tetfort, J. Carbeck and G. Whitesides, *Science*, 1997, **276**, 233–235.
34 M. Nicolson, *Proc. Cambridge Philos. Soc.*, 1949, **45**, 288–295.
35 D. Vella and L. Mahadevan, *Am. J. Phys.*, 2005, **73**, 817–825.
36 M. Nikolaides, A. Bausch, M. Hsu, A. Dinsmore, M. Brenner, C. Gay and D. Weitz, *Nature*, 2002, **420**, 299–301.
37 E. Van Nierop, M. Stinjman and S. Hilgenfeld, *Europhys. Lett.*, 2005, **72**, 671–677.
38 D. Stamous and C. Duschl, *Phys. Rev. E: Stat. Phys., Plasmas, Fluids, Relat. Interdiscip. Top.*, 2000, **62**, 5263–5271.
39 A. Würger, *Phys. Rev. E: Stat., Nonlinear, Soft Matter Phys.*, 2006, **74**, 041402.

 This journal is © The Royal Society of Chemistry 2014